DYNAMICS OF PRESTRESSED ROTATING ANISOTROPIC PLATES SUBJECT TO TRANSVERSE LOADS AND HEAT SOURCES, PART II: APPLICATION TO A SPECIALLY ORTHOTROPIC DISK

Heuigi Son[†], Noboru Kikuchi, A. Galip Ulsoy and Ahmet S. Yigit[‡]

Department of Mechanical Engineering and Applied Mechanics, University of Michigan, Ann Arbor, MI 48109-2125, U.S.A.

The rotating disk has many engineering applications as in floppy, hard, compact, laser, and recently optical disk drives. This paper (Part II) considers the application of a finite element method presented in a companion paper (Part I) to the analysis of rotating disks. The critical speed of the disk is obtained to validate the problem formulation and solution method. Dynamic responses are obtained as parameterized by the rotating speed. Effects of the temperature distribution and material system are also observed. Thermal effects are crucial in the analysis of rotating disks, since the variation of temperature can be significant. This is especially true for equipment in which a heat source is used as a means of recording or erasing data and for equipment in which the amount of generated or transferred heat is significant. The specially orthotropic material properties of a laminated disk can have a large effect on the overall dynamic behavior.

© 2000 Academic Press

1. INTRODUCTION

This paper (Part II) considers the application of the finite element method, as presented in a companion paper (Part I), to the dynamic analysis of rotating disks. The effects of transverse forces, heat sources, and orthotropic material properties are considered.

   In section 2, the dynamics of a rotating disk is analyzed for several materials typical of a floppy disk, and an aluminum annular plate. Critical speeds are obtained for verification of the finite element formulation. In section 3, optical disks are studied. Dynamic responses and the natural frequencies are obtained for both the cases where the temperature effects are ignored and considered. It is shown that the temperature distribution is very important in the analysis of an optical disk. One way of reinforcing optical disks is by using a laminate composed of the material of the optical disk and of aluminum. Not only is such a laminate far stiffer than typical optical disks, but the thermal effect on the dynamics of a rotating disk becomes remarkably reduced. The specially orthotropic material properties are obtained based upon the homogenization method and used for the simulation of the dynamics of laminated disks. This is an important application problem in its own right, and a special case of general theory developed in Part I. Finally, section 4 contains the conclusions.

[†] Currently with Goldstar Corp.
[‡] On leave from Kuwait University.

© 2000 Academic Press

2. DYNAMICS OF A ROTATING DISK

The dynamics of rotating disks are considered here. The configuration of the disk and the problem are illustrated in Figure 1 in part I, where R_o and R_i are the outer and inner radii, and h is the thickness.

The critical speed for divergence instability is obtained for the system matrices obtained by the software developed here for the purpose of verification. Since the consistent stiffness matrix and damping (gyroscopic) matrix already contain the contributions of the geometric body forces at a given state (see Part I, Appendix A), it is possible to obtain the eigenvalues as parameterized by the rotating speed of the disk.

The second order ordinary differential equations of the form

$$\mathbf{M\ddot{x} + G\dot{x} + Kx = 0} \tag{1}$$

are transformed into state-space form as follows:

$$\dot{\mathbf{y}} = \mathbf{Ay}, \qquad \mathbf{A} = \left[\begin{array}{c|c} \mathbf{0} & \mathbf{I} \\ \hline -\mathbf{M}^{-1}\mathbf{K} & -\mathbf{M}^{-1}\mathbf{G} \end{array} \right], \qquad \mathbf{y} = \left\{ \begin{array}{c} \mathbf{X} \\ \dot{\mathbf{X}} \end{array} \right\}. \tag{2}$$

The eigensystem subroutine package *eispack* is utilized. For a plate problem, the mass matrix and stiffness matrix has elements of $O(h)$ and $O(h^3)$. This causes the problem of a large condition number. To avoid numerical problems associated with the large condition number, balancing is done before obtaining the eigenvalues.

The critical speeds of rotating disks were computed and compared to published results for two special cases. Consider a floppy disk having the following properties and dimensions: $E = 4.9$ GPa, $v = 0.33$, $\rho = 1300$ kg/m^3, $h = 7.8 \times 10^{-5}$ m, $R_o = 0.1$ m, $R_i = 0.025$ m; and a saw blade having the following properties and dimensions: $E = 193$ GPa, $v = 0.33$, $\rho = 7870$ Kg/m^3, $h = 1.65 \times 10^{-3}$ m, $R_o = 0.305$ m, $R_i = 0.043$ m.

The boundary conditions are chosen such that the disk is clamped along the inner radius, $r = R_i$, and free along the outer radius, $r = R_o$. Chonan [1] has shown that the critical speeds for the floppy disk and the saw blade are 230 r.p.m. (theoretically), and 1100 r.p.m. (experimentally) respectively. In this study, a 64-element discretized domain, as illustrated in Figure 1, is used in computing the eigenvalues. The critical rotational speeds are defined as
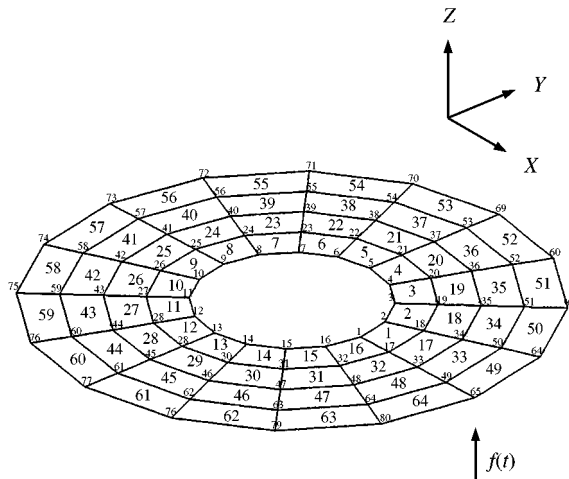

Figure 1. 64-Element disk problem.

TABLE 1

Comparison of non-dimensional natural frequencies

	Mode [m, n]					
	[0, 0]	[0, 1]	[0, 2]	[0, 3]	[0, 4]	[0, 5]
Our results	12·86880	13·07891	14·15186	17·29894	23·99848	35·88012
Mote [2]	13·02426	13·28978	14·70381	18·56195	25·59583	35·73003

the rotating speeds when the imaginary part of an eigenvalue becomes zero while the real part of the eigenvalue remains zero (i.e., divergence instability). The first critical speed is computed as 234·7 r.p.m. for the floppy disk and 1139·7 r.p.m. for the sawblade respectively. Those values agree to within 4% with those reported by Chonan [1].

For a stationary disk when the ratio of the inner radius to the outer radius is 0·5, the natural frequencies were computed and compared to published data [2]. Results were obtained using the following material properties and dimensions: $E = 65·5$ MPa, $v = 0·3$, $\rho = 1200$ kg/m^3, $h = 0·0012$ m, $R_o = 0·065$ m, $R_i = 0·0325$ m.

The computed natural frequencies are compared in Table 1. Here mode [m, n] denotes the mode with m nodal circles and n nodal lines. The non-dimensional natural frequency, Φ, is computed from the natural frequency, ω, using the relation

$$\Phi = \left[\frac{\rho h R_o^4}{D_o} \right]^{1/2} \omega,$$

where

$$D_o = \frac{Eh^3}{12(1 - v^2)}.$$

The maximum error between the results obtained here and those obtained by Mote is 7% [2].

3. DYNAMICS OF OPTICAL DISKS

The first generation of optical disk drives produced were read-only (RO) disk drives, where heat sources are used only once for storing data at a factory, and optical heads are used for reading data. Since an optical head is well away from the surface of the disk, the interaction force between the disk and head may not be important in this case. The next generation of optical disk drive is of the write-once-read-many-times (WORM) type in which the heat source is used once at the user location to store data, and an optical head is used for reading data. The latest type is an erasable optical disk drive utilizing a disk as in hard disk drives. The magnetic-optical disk is most suitable in the application of the erasable optical disk [3], where both heat sources and magnetic heads or optical heads may be used. The analysis of such optical disk drives needs to include the effects of both space-fixed transverse forces and heat sources. There are several different standard dimensions available for optical disks. For all cases, the thickness of single-sided optical disks is 1·2 mm and that of double-sided optical disks is twice as much, or 2·4 mm. Here, the case when the thickness is 1·2 mm is considered. The material widely used as the substrate for optical disks is an optical grade of polycarbonate (PC), polymethylmethacrylate

(PMMS), or glass. It is also proposed in this study to use a laminated disk with an aluminum layer to improve the dynamic response. First, the dynamics of an isotropic disk made of a substrate of an optical grade of polycarbonate (PC) will be presented.

3.1. DYNAMICS OF AN ISOTROPIC DISK

Here the model for the optical disk is chosen as C-130SR grade, which is typical of optical disks in current use. The outer radius is 65 mm and the inner clamping radius is chosen as 15 mm. The surface of the optical disk has many pits, or grooves, along the data tracks which are covered by several layers. But the depths of the grooves or the thickness of the layers except the substrate are so tiny (0·06–0·12 μm, or 250–800 Å) that the existence of those grooves or layers does not affect the global material properties to a significant level. Therefore, it is assumed that the material properties are the same as a disk made solely of the substrate material (PC) of full thickness. The corresponding material properties and the dimensions of the optical disk of interest are listed in Table 2.

The lowest 10 natural frequencies and their mode shapes for the stationary optical disk are obtained as shown in Table 3. The real parts and the imaginary parts of the eigenvalues for various rotational speed are obtained as in Figure 2. As can be seen in Figure 2, the [0, 2] mode shows the first critical speed [divergence instability) at a speed of $\Omega = 112·5$ rad/s or 1070 r.p.m. When the disk is rotating at a speed different than the critical speeds, not exceeding the critical speed for flutter instability, the disk is stable, because the real parts of the eigenvalues remain zero, and the imaginary parts are positive.

If the rotation speed becomes larger, then some travelling wave frequencies coalesce. In this case, the travelling waves of the [0, 4] and [0, 5] modes are shown to meet at $\Omega = 265$ and at 268·8 rad/s respectively. Once the rotation speed exceeds this flutter critical speed, the disk becomes unstable, because the eigenvalue of the related modes has positive real parts as shown in Figure 2.

It is clear that this optical disk made of a plastic substrate is not sufficiently stiff. The first critical speed is $\Omega = 112·5$ rad/s or 1070 r.p.m. Considering the trend that the rotational speed in disk drives continues to increase (e.g., 1800–2400 to 3000–3600 r.p.m.), this critical speed is very low.

The impulse response and step response are both obtained for various rotation speeds, and illustrated in Figures 3–7. It is noted that at the divergence critical speed, the impulse

TABLE 2

Material properties and dimensions of optical disk

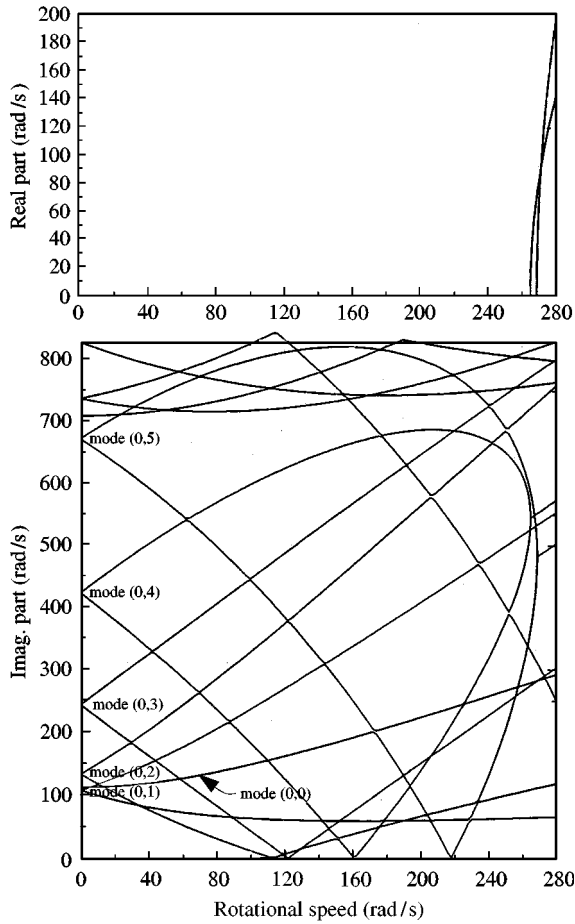| Item	Symbol	Unit	PC
Young's modulus	E	Pa	$65·5 \times 10^6$
Shear modulus	G	Pa	$25·2 \times 10^6$
Poisson's ratio	v	—	0·3
Density	ρ	kg/m^3	1200
Heat capacity	ρc_p	J/m^3 °K	$1·51 \times 10^6$
Thermal conductivity	k	W/m °K	0·0159
Thermal expansion coefficient	α	m/m °K	$67·5 \times 10^{-6}$
Thickness	t	m	0·012
Inner radius	R_i	m	0·015
Outer radius	R_0	m	0·065

Figure 2. Real and imaginary parts of eigenvalues versus rotational speed.
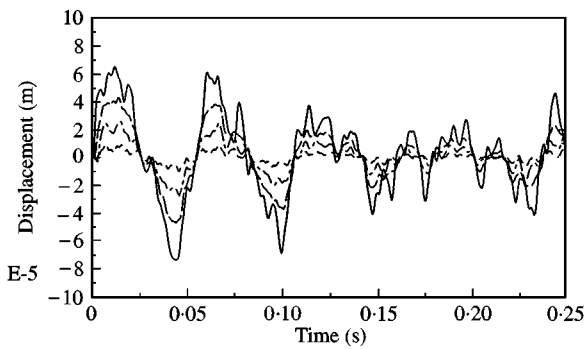

Figure 3. Transverse deflection of optical disk ($\Omega = 0$): – – –, node 17; – · –, node 33; — —, node 49; ——, node 65.

response as in Figure 4 is bounded, while the forced response to a step input is divergent as in Figure 5.

The response when $\Omega = 263$ rad/s is stable, while that of $\Omega = 264$ rad/s diverges as shown in Figures 6 and 7. Figure 6 shows a beating phenomenon, because the two frequencies are very close to each other. This can be verified by examining Figure 2. Two travelling waves
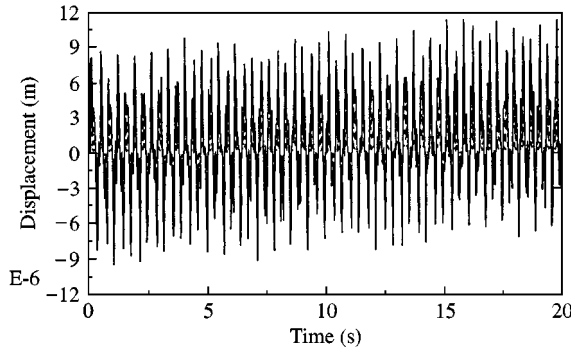
Figure 4. Transverse deflection of optical disk ($\Omega = 112 \cdot 5$ rad/s); key as for Figure 3.
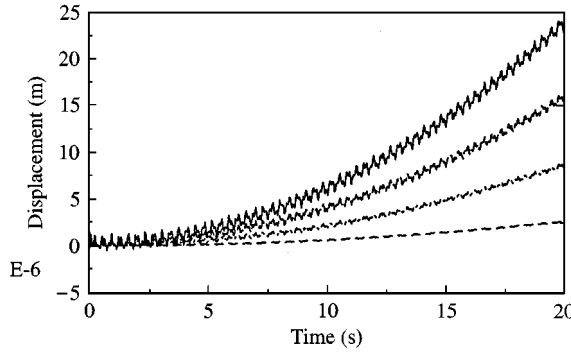

Figure 5. Transverse deflection of optical disk (step force and $\Omega = 112 \cdot 5$ rad/s); key as in Figure 3.
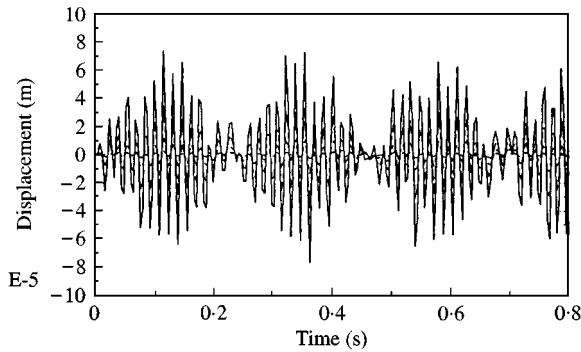

Figure 6. Transverse deflection of optical disk ($\Omega = 263$ rad/s); key as for Figure 3.

almost coalesce when $\Omega = 263$, therefore, the beating phenomenon occurs. However, at $\Omega = 264$ rad/s the real part of the eigenvalue for this [0, 4] mode becomes positive, leading to a flutter instability.

Next, consider the effect of a heat source on the dynamic response of the disk. There may be some difficulties, due to very different time constants between temperature and dynamic deflections, in clearly assessing the effect of temperature distribution on the dynamics of the rotating disk. It usually takes a long time for the temperature distribution to reach its steady state, while the mechanical dynamics of the disk is very fast.
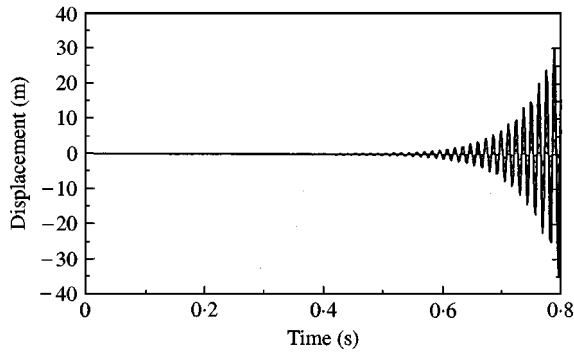
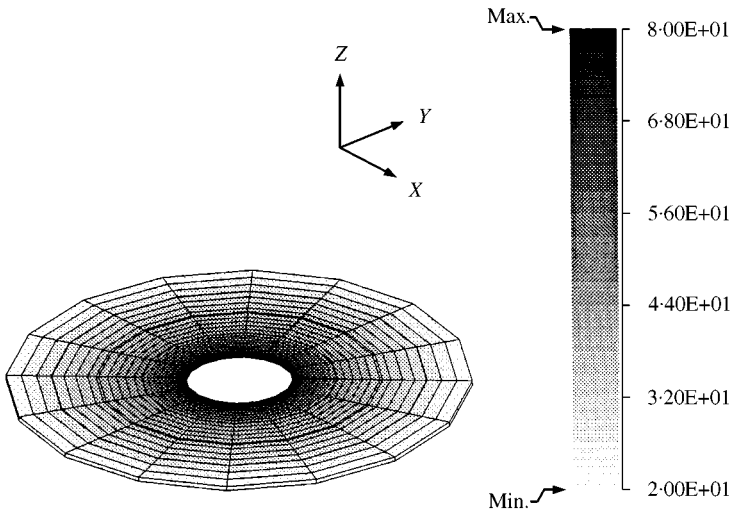Figure 7. Transverse deflection of optical disk ($\Omega = 264$ rad/s); key as for Figure 3.

Figure 8. Initial temperature distribution of optical disk.

The following approach was used in this study to consider the effects of temperature distribution in the analysis [4]. First, the thermal and bending problems are uncoupled and the temperature distribution, having a large time constant, is obtained using larger time increments until it reaches an equilibrium. During this stage the computation of the in-plane or out-of-plane responses is almost meaningless, because the time increment is too large for the accuracy of the dynamic deflections. Hence, the deformations are assumed to be zero and the effect of deflection on the temperature distribution is neglected during this stage. Then, the temperature distribution is used as an initial temperature distribution, and the coupled thermal and plate bending problems are solved. In this way, one can circumvent having to integrate over a sufficiently small time increment enough to accurately catch the history of deflections, during the long time period when the temperature reaches its equilibrium or near equilibrium state.

Here, the temperature at the inner radius was specified as increased by 80°C and that at the outer radius was specified as increased by 20°C. Since the time constant for the thermal problem is very large, it is necessary to integrate for a long time to get a converged temperature distribution. The temperature distribution over the domain at the converged state ($t = 2 \times 10^5$ s) is illustrated in Figure 8, and the time history of temperature at several
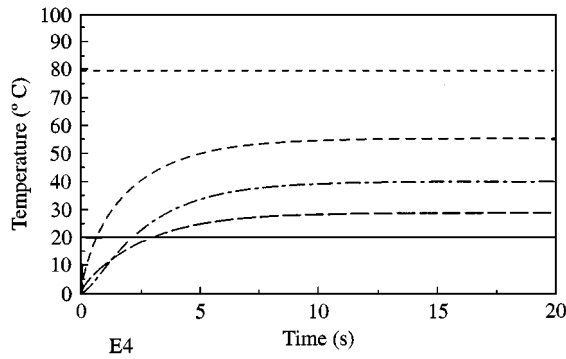
Figure 9. Time history of temperature of optical disk ($\Omega = 0$): - - -, node 1; – – –, node 17; – · –, node 33; — — , node 49; ——, node 65.

TABLE 3

Comparison of natural frequencies for an optical disk and a prestressed disk

	Optical disk			Prestressed disk	
Mode	Mode shape	Frequency	Mode	Mode shape	Frequency
1/2	[0, 1]	1.067627E + 02	1	[1, 0]	7.640946E + 02
3	[1, 0]	1.115264E + 02	2/3	[0, 1]	8.881420E + 02
4/5	[0, 2]	1.326079E + 02	4/5	[0, 2]	1.981739E + 02
6/7	[0, 3]	2.427173E + 02	6/7	[0, 3]	3.466040E + 02
8/9	[0, 4]	4.230415E + 02	8/9	[0, 4]	5.395710E + 02
10	[0, 5]	6.720320E + 02	10	[2, 0]	6.716963E + 02

nodal points for a time period of $[0.2 \times 10^5]$ s is shown in Figure 9. It can be seen that the temperature reaches a steady state concentric temperature distribution. This temperature distribution is used as an initial condition for the study of the effect of initial temperature. Due to this initial temperature distribution there is a residual stress which affects the dynamic characteristics of the disk. The natural frequencies of optical disks and those of prestressed optical disks are compared in Table 3. The real parts and the imaginary parts of the eigenvalues for prestressed disks with varying rotational speed are obtained as in Figure 10. And their mode shapes are illustrated in Figure 11. It is shown that the first critical speed for the divergence instability is increased in the prestressed disk even though the lowest eigenvalue for the stationary case was lower than the unstressed optical disk. The first critical speed is 167 rad/s or 1590 r.p.m., which is well beyond the previous critical speed of 112·5 rad/s or 1070 r.p.m. The reason why the prestressed disk has the higher critical speed is interesting. Although the prestressed disk has the smaller lowest eigenvalues when $\Omega = 0$, those lowest mode frequencies tend to increase as the rotational speed increases. The first divergence critical mode is the [0, 2] mode for both the optical disk and the prestressed disk. Accordingly the eigenvalues of the [0, 2] modes for the prestressed disk and the optical disk affect the first critical speed. The eigenvalues of the [0, 2] mode of the prestressed disk are 1·49 times that of the unstressed disk, and the first divergence critical speed turns out to be 1·48 times that for the unstressed optical disk.

The impulse responses were obtained (not shown here) for various rotational speeds Ω, and show trends similar to those in Figures 3–7.
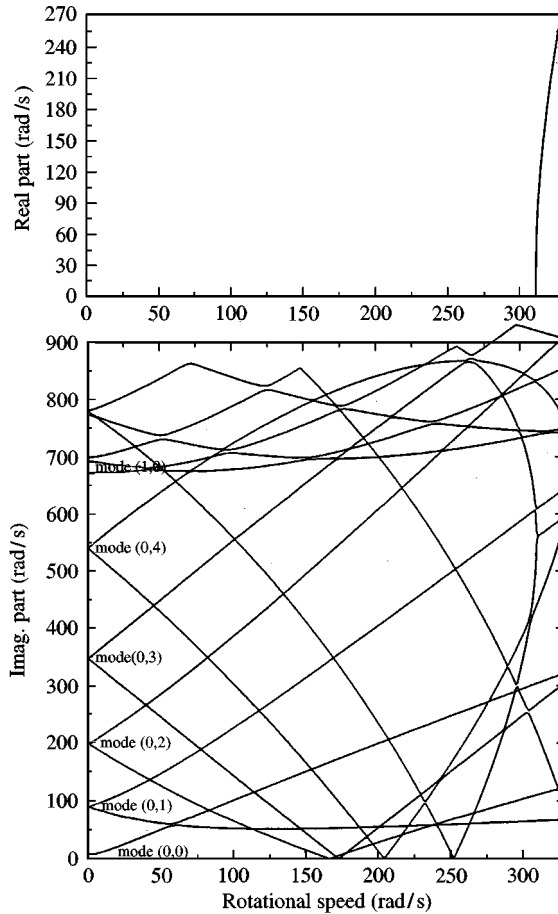
Figure 10. Real and imaginary parts of eigenvalues versus rotational speed for prestressed disk.

3.2. DYNAMICS OF A LAMINATED OPTICAL DISK

A disk of a laminate material composed of polycarbonate (PC) and aluminium layers is studied in this section. While a very thin aluminum layer of thickness 500–600 Å is usually coated onto optical disks, here the aluminum layer is chosen much thicker so that the effect of this layer on the dynamic behavior of a composite disk can be readily observed. Thus, the volume fraction of aluminum is chosen as 25%.

In order to obtain the material properties of this laminate, the homogenization method was used. Due to the simplicity of the material system used in this example, the rule of mixtures can also be used. In fact, the thermal properties of the laminated disk are obtained using a rule of mixture instead of the homogenization method. The material for each layer is assumed to be isotropic and homogeneous. The properties of the laminate are, however, specially orthotropic. Table 4 specifies the properties of the material for each layer.

The homogenized orthotropic elastic material properties obtained are $C_{1111} = C_{2222} = 17 \cdot 11$ GPa, $C_{1122} = C_{2211} = 5 \cdot 148$ GPa, $C_{1212} = C_{2121} = C_{1221} = C_{2112} = 5 \cdot 980$ GPa, $C_{1313} = C_{2323} = 0 \cdot 0336$ GPa, $C_{imjn} = 0$ otherwise.

By using the relations between the elasticity tensor and the directional material properties one can directly compute the directional properties: $v_{21} = C_{1122}/C_{1111}$,
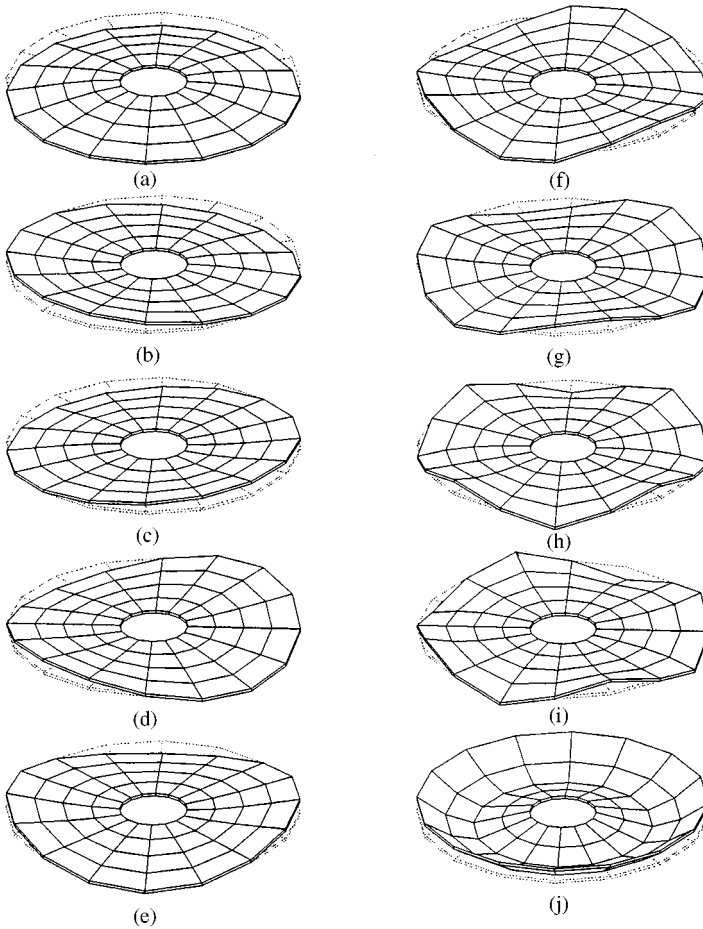
Figure 11. The lowest 10 mode shapes for prestressed disk: (a) [0, 0] mode, 7·6 rad/s; (b) [0, 1] mode, 89 rad/s; (c) [0, 1] mode, 91 rad/s; (d) [0, 2] mode, 198 rad/s; (e) [0, 2] mode, 199 rad/s; (f) [0, 3] mode, 347 rad/s; (g) [0, 3] mode, 347 rad/s; (h) [0, 4] mode, 540 rad/s; (i) [0, 4] mode, 540 rad/s; (j) [1, 0] mode, 672 rad/s.

TABLE 4

Materials properties of raw materials

Item	Symbol	Unit	PC	Aluminum
Young's modulus	E	Pa	$65\cdot5 \times 10^6$	$62\cdot0 \times 10^9$
Shear modulus	G	Pa	$25\cdot2 \times 10^6$	$24\cdot0 \times 10^9$
Poisson's ratio	v	—	$0\cdot3$	$0\cdot3$
Density	ρ	kg/m^3	1200	2700
Thickness	t	m	$0\cdot009$	$0\cdot003$
Heat capacity	ρc_p	J/m^3 °K	$1\cdot51 \times 10^6$	$2\cdot44 \times 10^6$
Thermal conductivity	k	W/m °K	$0\cdot0159$	237
Thermal expansion coefficient	α	m/m °K	$67\cdot5 \times 10^{-6}$	22×10^{-6}

$v_{12} = C_{2211}/C_{2222}$, $v^2 = v_{12}v_{21}$, $E_1 = (1 - v^2)C_{1111}$, $E_2 = (1 - v^2)C_{2222}$, $G_{12} = C_{1212}$, $G_{13} = C_{1313}$, $G_{23} = C_{2323}$.

The orthotropic thermal conductivities and thermal expansion coefficient of the composite were obtained by using the rule of mixtures and are given in Table 5.

Material properties of composite material

Item	Symbol	Unit	A1 25% + PC
Young's modulus	E_1	GPa	15·56
	E_2	GPa	15·56
Shear modulus	G_{12}	GPa	5·980
	G_{13}	GPa	0·03358
	G_{23}	GPa	0·03358
Poisson's ratio	v_{12}	—	0·3009
	v_{21}	—	0·3009
Density	ρ	kg/m^3	1575
Thickness	t	m	0·0012
Heat capacity	ρc_p	MJ/m^3 °K	1·740
Thermal conductivity	k_{11}	W/m °K	59·26
	k_{22}	W/m °K	59·26
Thermal expansion coefficient	α_{11}	m/m °K	$0·213 \times 10^{-6}$
	α_{22}	m/m °K	$0·213 \times 10^{-6}$

The lowest 10 mode shapes were obtained for this laminated disk. Figure 12 shows the mode shapes of this laminated disk, but some mode shapes look quite unusual. The fourth, seventh, and eighth mode shapes show that some elements are very highly deformed. Such severe deformations must generate a high strain energy within the body. Accordingly those modes, if they are in fact mode shapes, should have eigenvalues of very large magnitudes. Actually they posses an "w-hourglass mode", which is the result of applying the selective reduced integration scheme in the integration of the four-node bilinear plate element based on Mindlin plate theory. The rank deficiency due to this reduced integration method is fixed by a special procedure for interpolating the transverse shear strains [5]. The scheme uses a "correct-rank, four-node bilinear element". Using this element, the lowest 10 mode shapes are correctly obtained as shown in Figure 13.

The first divergence critical speed of this laminated disk is 2890 rad/s, or 27 600 r.p.m. Thus, it can be said that this kind of disk can withstand the high rotational speeds typical of a high speed disk drive. The transverse deflection versus time has been obtained when the rotation speed of the disk is 377 rad/s, or 3600 r.p.m. and is shown in Figure 14.

In order to consider the effect of a heat source on the transverse deflection, first the thermal and bending problems are decoupled and the temperature distributions after $t = 400$ s with the rotational speed of 377 rad/s (3600 r.p.m.) or 2891 rad/s (27 600 r.p.m.) are obtained. This temperature distribution is then used as an initial condition. Here, the temperature at the clamped radius is specified as being increased by 80°C, and the outer radius is specified as being increased by 20°C, and the temperature of the ambient air is 0°C. The time histories of temperature during this time period at several nodes are shown in Figures 15 and 16. Notice that the temperature distribution inside the domain, for the case with $\Omega = 2891$ rad/s, becomes lower due to the larger heat convection coefficients for larger rotational speed. The first divergence critical speed for this case is 2891 rad/s, which is very close to the critical speed 2890 rad/s for the case without thermal effect. The impulse responses are obtained at the rotational speed of 3600 r.p.m. in Figure 17.
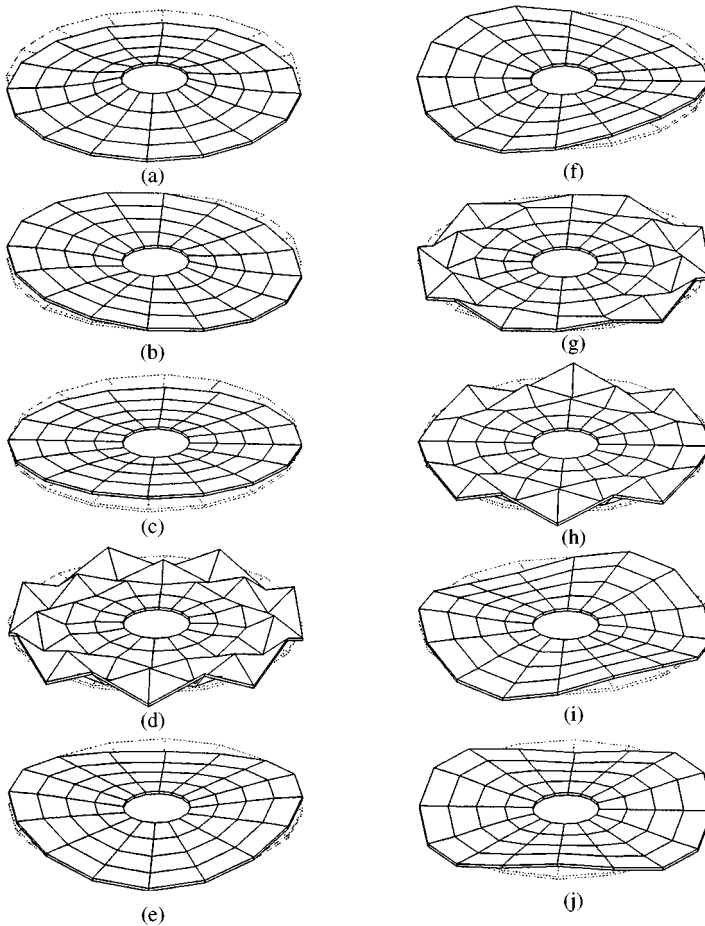
Figure 12. The lowest 10 mode shapes for laminated disk (without hourglass control): (a) [0, 0] mode, 966×10^6 rad/s; (b) [0, 1] mode, 133×10^7 rad/s; (c) [0, 1] mode, 133×10^7 rad/s; (d) hourglass, 165×10^7 rad/s; (e) [0, 2] mode, 316×10^7 rad/s; (f) [0, 2] mode, 316×10^7 rad/s; (g) hourglass, 317×10^7 rad/s; (h) hourglass, 317×10^7 rad/s; (i) [0, 3] mode, 575×10^7 rad/s; (j) [0, 3] mode, 575×10^7 rad/s.

It was shown that the optical disk studied in the preceding section was greatly affected by temperature. In this laminated disk case, however, the effect of temperature is remarkably reduced.

The very general formulation in Part I enables one to include any complex temperature distribution in the analysis of the dynamic deflections. To emphasize this capability, a case when a temperature distribution is not axisymmetric is considered. Here the temperature at the inner radius was specified as increased by 60–80°C and that at the outer radius was specified as increased by 20–40°C. The temperature distribution over the domain at the converged state ($t = 200$ s) is illustrated in Figure 18, and the time history of temperature at several nodal points for a time period of [0, 200] s is shown in Figure 19. The real parts and the imaginary parts of the eigenvalues for prestressed disks with varying rotational speed are obtained as in Figure 20. The mode shapes are illustrated in Figure 21. Since the effect of temperature on the dynamic deflections is very small in this laminated disk case, the effect of non-symmetric temperature distribution is small too. The first divergence critical mode is the [0, 8] mode.
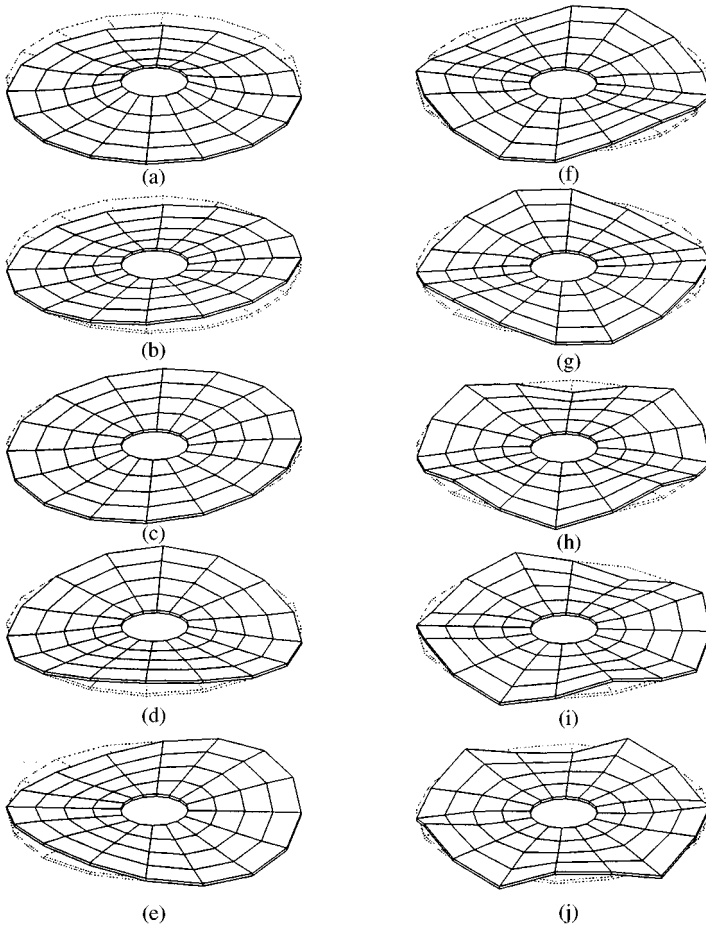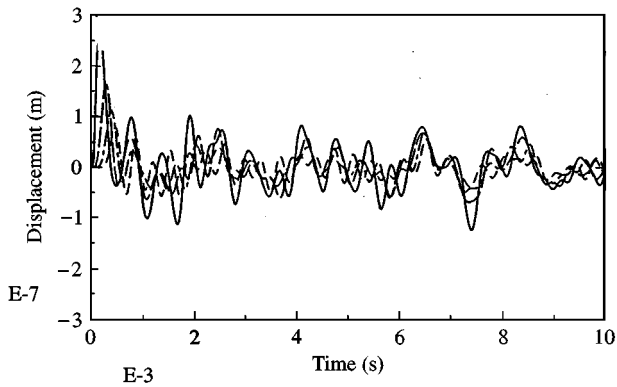
Figure 13. The lowest 10 mode shapes for laminated disk (with hourglass control): (a) $[0, 0]$ mode, $9 \cdot 63 \times 10^6$ rad/s; (b) $[0, 1]$ mode, $1 \cdot 33 \times 10^7$ rad/s; (c) $[0, 1]$ mode, $1 \cdot 33 \times 10^7$ rad/s; (d) $[0, 2]$ mode, $3 \cdot 13 \times 10^7$ rad/s; (e) $[0, 2]$ mode, $3 \cdot 13 \times 10^7$ rad/s; (f) $[0, 3]$ mode, $5 \cdot 71 \times 10^7$ rad/s; (g) $[0, 3]$ mode, $5 \cdot 71 \times 10^7$ rad/s; (h) $[0, 4]$ mode, $8 \cdot 25 \times 10^7$ rad/s; (i) $[0, 4]$ mode, $8 \cdot 25 \times 10^7$ rad/s; (j) $[0, 5]$ mode, $1 \cdot 03 \times 10^8$ rad/s.

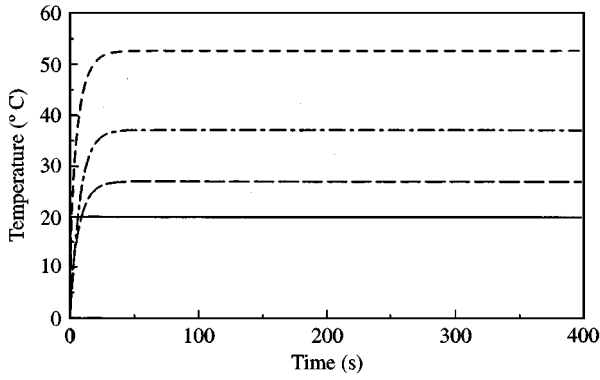Figure 14. The transverse deflection of laminated disk ($\Omega = 377$ rad/s); key as for Figure 3.

Figure 15. Time history of temperature of laminated disk ($\Omega = 377$ rad/s); key as for Figure 3.

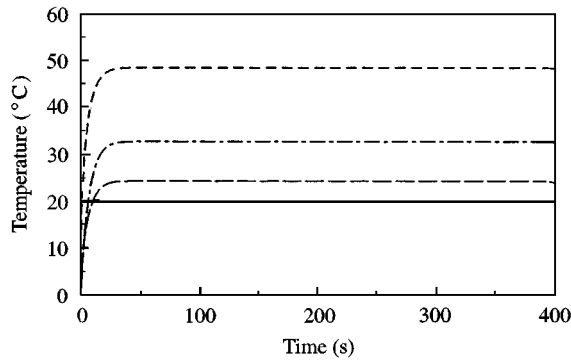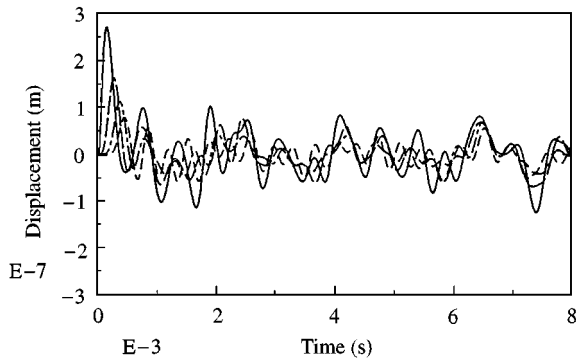Figure 16. Time history of temperature of laminated disk ($\Omega = 2891$ rad/s); key as for Figure 3.

Figure 17. Impulse response of prestressed laminated disk, key as for Figure 3.

4. SUMMARY AND CONCLUSIONS

This paper utilizes a finite element approach, described in detail in reference [4], to investigate the effects of transverse loads, prestresses and heat sources on the dynamics of rotating specially orthotropic disks.
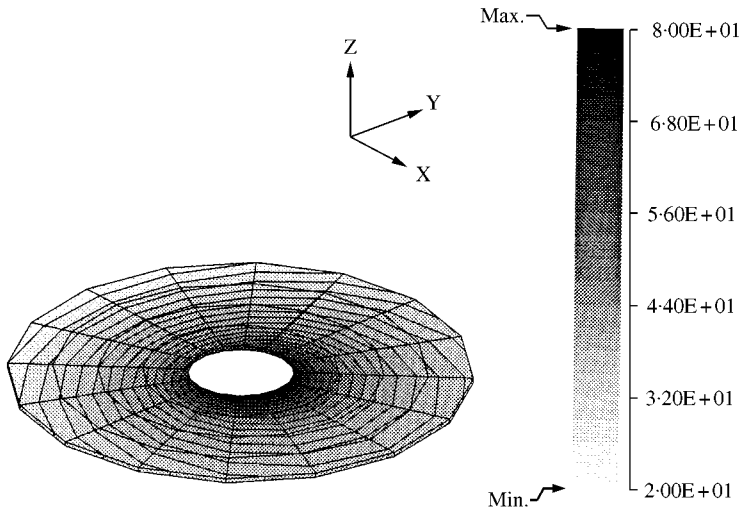
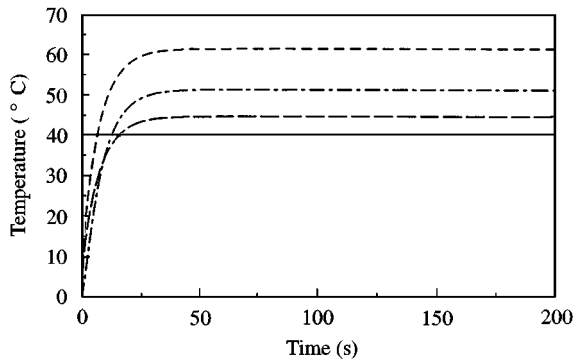Figure 18. Initial temperature distribution of laminated disk.

Figure 19. Time history of temperature of laminated disk, key as for Figure 3.

A case study for optical disks was done in detail. Isotropic material properties were assumed for the first example. The eigenvalues and the corresponding mode shapes as parametrized by the rotational speed were obtained. It was shown that in most cases, the two nodal line mode [0, 2] was the mode that results in the first divergence critical speed. The time responses are shown at various rotational speeds. The divergence instability and the flutter instability were observed through the time responses. Also the beating phenomenon was shown and explained. In order to observe the effect of a temperature gradient on the dynamics of rotating disks, an initial temperature distribution was obtained and used. This prestressed disk showed different eigenvalues than the unstressed disk, and the choice of the initial temperature distribution happens to increase the magnitude of the first divergence critical speed and the first flutter critical speed significantly.
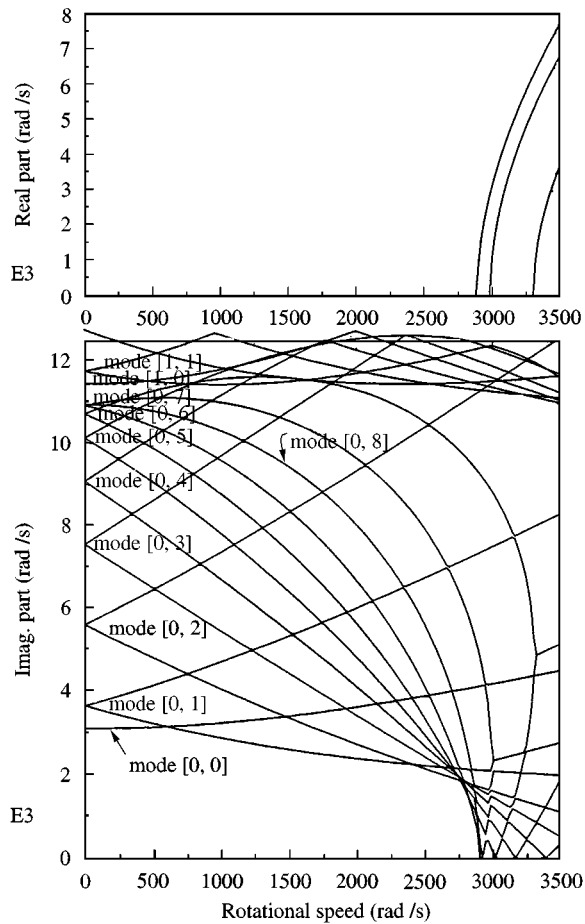
Figure 20. Real and imaginary parts of eigenvalues versus rotational speed for prestressed laminated disk.

A laminated optical disk, which reinforces the conventional optical disk with a thin aluminum layer, was studied. This laminated disk has a 25% volume fraction of aluminum. The homogenization method and the averaging methods were used to compute the orthotropic elastic and thermal material properties of the laminated disk. The *w*-hourglass control effect is shown in this study. This choice of the laminated disk showed an increase of the first divergence critical speed of 26 times. A temperature gradient similar to the one considered previously is initially given to the laminated disk and it was shown that the effect of temperature was remarkably reduced.

The conclusions of this research can be summarized as follows: (1) The temperature gradient can significantly change the dynamics of disks, especially for the case of optical disks, where the material is weak and the thermal expansion coefficient is large. (2) The orthotropic material properties of the laminated disk can have a large effect on the overall dynamics of disks. The laminated disk chosen in this study increases the first divergence critical speed significantly and reduces the effect of temperature on the deflection.
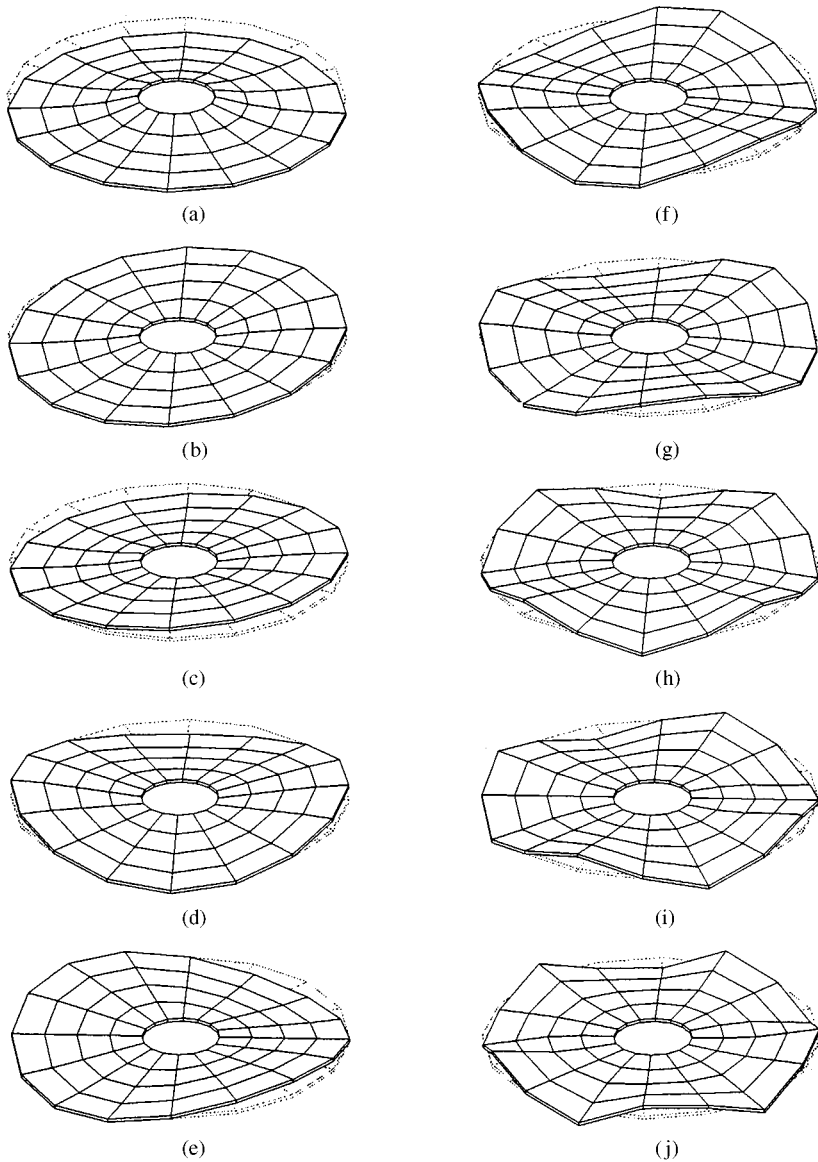
Figure 21. The lowest 10 node shapes of prestressed laminated disk: (a) [0, 0] mode, $3 \cdot 10 \times 10^3$ rad/s; (b) [0, 1] mode, $3 \cdot 64 \times 10^3$ rad/s; (c) [0, 1] mode, $3 \cdot 64 \times 10^3$ rad/s; (d) [0, 2] mode, $5 \cdot 60 \times 10^3$ rad/s (e) [0, 2] mode, $5 \cdot 60 \times 10^3$ rad/s; (f) [0, 3] mode, $7 \cdot 56 \times 10^3$ rad/s; (g) [0, 3] mode, $7 \cdot 56 \times 10^3$ rad/s; (h) [0, 4] mode, $9 \cdot 08 \times 10^3$ rad/s; (i) [0, 4] mode, $9 \cdot 08 \times 10^3$ rad/s; (j) [0, 5] mode, $1 \cdot 01 \times 10^4$ rad/s.

REFERENCES

1. S. CHONAN 1987 *Journal of Applied Mechanics* **54**, 967–968. On the critical speed of a rotating circular plate.
2. C. D. MOTE JR. 1977 *Journal of the Acoustic Society of America* **61**, 439–447. Moving-load stability of a circular plate on a floating central collar.
3. Y. TOGAMI 1982 *IEEE Transactions on Magnetics* **MAG-18**, 1233–1237. High performance substrate for magneto-optical disk.

4. H. SON, N. KIKUCHI, A. G. ULSOY and A. S. YIGIT 2000 *Journal of Sound and Vibration.* Dynamics of prestressed rotating anisotropic plate subject to transverse loads and heat sources, Part I; modeling and solution method. (to appear)

5. T. J. R. HUGHES and T. E. TEZDUYAR 1981 *Journal of Applied Mechanics* **48**, 587–596. Finite elements based upon mindlin plate theory with particular reference to the four-node bilinear isoparametric element.